Available online at www.sciencedirect.com
SCIENCE DIRECT®
International Journal of Mass Spectrometry 234 (2004) 89–99
International Journal of Mass Spectrometry
www.elsevier.com/locate/ijms

Fragmentation energetics for angiotensin II and its analogs from time- and energy-resolved surface-induced dissociation studies

Julia Laskin [a,*], Thomas H. Bailey [b], Jean H. Futrell [a]

[a] *Pacific Northwest National Laboratory, Fundamental Science Directorate, P.O. Box 999 (K8-88), Richland, WA 99352, USA*
[b] *Department of Chemistry and Biochemistry, University of Delaware, Newark, DE 19716, USA*

Received 18 November 2003; accepted 4 February 2004

Abstract

Surface-induced dissociation (SID) of four model peptides: DRVYIHPF, RVYIHPF, RVYIHAF, and RVYIHDF was studied using a novel Fourier transform ion cyclotron resonance mass spectrometer (FT-ICR MS) specially configured for SID experiments. The energetics and dynamics of peptide fragmentation were deduced by modeling the time- and energy-resolved survival curves for each precursor ion using an RRKM based approach developed in our laboratory. Accurate dissociation parameters can be obtained from these experiments because collision-energy-resolved SID data are very sensitive to both the energetics and dynamics of dissociation. We found that transition from selective to non-selective fragmentation as ion kinetic energy is increased is associated with a substantial (ca. 0.5 eV) increase in the dissociation energy and a 3–4 orders of magnitude increase in the pre-exponential factor. Dissociation thresholds for angiotensin analogs derived from the experimental data are as follows: 1.62 eV for RVYIHAF and RVYIHPF, 1.14 eV for RVYIHDF and 1.13 eV for DRVYIHPF. Pre-exponential factors of 8.2×10^{11}, 7.2×10^{12}, 3.1×10^{8}, and 5.0×10^{7} s^{-1} were obtained for RVYIHPF, RVYIHAF, RVYIHDF, and DRVYIHPF, respectively. Contribution from shattering to the total decomposition of the precursor ion increases for kinetically hindered fragmentation. The largest contribution is observed for a peptide ion that has the largest negative reaction entropy—DRVYIHPF.

Keywords: Surface-induced dissociation; RRKM modeling; Protonated peptides; Fragmentation energetics; Reaction entropy; FT-ICR MS; Selective cleavage

1. Introduction

Gas-phase dissociation of peptide ions has been utilized in a large number of mass spectrometric studies focused on structural characterization and identification of peptides and proteins using tandem mass spectrometry (MS/MS). A general model describing dissociation of peptide ions has emerged [1–7]. This model asserts that protons are transferred intramolecularly from the initial protonation site of the peptide to carbonyl oxygens along the backbone in order to initiate backbone cleavages. The electropositive carbon of the protonated carbonyl is then attacked by a nearby N-terminal carbonyl group leading to cleavage of the peptide backbone close to the protonation site. It has also been suggested that basic residues of the peptide can sequester the proton. Consequently, for peptides containing basic residues such as arginine, lysine or histidine higher energy is required to "mobilize" the proton to make it available for backbone fragmentation.

Peptide ions that contain both acidic (aspartic or glutamic acid) and basic residues undergo very specific fragmentation when the number of protons does not exceed the number of basic residues [8]. Preferential cleavage of peptide backbone C-terminal to the acidic residue has been studied by several groups [8–12]. Two different mechanisms for selective cleavages at acidic amino acid residues when arginine is present in the peptide sequence have been proposed. The charge-directed mechanism proposed by Gaskell and co-workers [11] suggests that interaction of the protonated guanidino group of arginine residue with the carboxyl group of the acidic residue results in the deprotonation of the acidic side chain, followed by proton transfer to the amide nitrogen C-terminal to the acidic residue. The resulting structure is stabilized via a strong electrostatic interaction between the protonated guanidino group and deprotonated carboxylic group. Proton transfer weakens

* Corresponding author. Tel.: +1-509-376-4443; fax: +1-509-376-3650.
E-mail address: Julia.Laskin@pnl.gov (J. Laskin).

1387-3806/$ – see front matter © 2004 Elsevier B.V. All rights reserved.
doi:10.1016/j.ijms.2004.02.022

the adjacent amide bond leading to facile fragmentation C-terminal to the acidic residue. Wysocki and co-workers [8,12] have proposed an alternative charge–remote mechanism. According to this mechanism interaction between the acidic and basic side chains results in charge solvation, while fragmentation preferentially occurs at acidic residues not involved in charge solvation.

Although gas phase fragmentation of peptide ions has been extensively studied phenomenologically, little is known on the energetics and dynamics of peptide fragmentation and their dependence on the presence of acidic and basic residues in the peptide. Detailed studies of this kind are hindered by difficulties in deriving accurate energetics and dynamics of peptide fragmentation from mass spectral data. The major obstacle for data interpretation is the presence of a large kinetic shift (KS) [13], defined as the internal energy in excess of the dissociation threshold required to produce detectable dissociation of a polyatomic ion on the timescale of a mass spectrometer, for complex molecules. Consequently quantitative analysis of dissociation of large ions requires statistical modeling of the microcanonical rate constants. This can be done using the RRKM/QET or the phase space theory (PST) [14].

We have recently developed an RRKM-based approach for analysis of collision-energy-resolved fragmentation of large ions excited by multiple collisions in the gas phase or by collisions with surfaces [15,16]. This approach has been extensively utilized for analysis of multiple-collision activation (MCA-CID) and surface-induced dissociation (SID) of ions in a Fourier transform ion cyclotron resonance mass spectrometer (FT-ICR MS) [17–20]. We found that the sensitivity of RRKM modeling to dissociation parameters can be significantly improved when collision-energy-resolved data is acquired at different reaction times. Time-resolved survival curves for the precursor ion are obtained by varying ion collision energy and reaction time and plotting the relative abundance of the precursor ion as a function of collision energy for each fragmentation delay. Reaction times that can be reliably explored using SID in the FT-ICR MS in our laboratory vary from 1 ms to many seconds.

We have recently conducted a detailed investigation of the energetics of selective cleavages at acidic residues by examining time- and energy-resolved fragmentation of four peptides that vary in the content and relative position of an arginine residue (LDIFSDF, LDIFSDFR, RLDIFSDF, LEIFSEFR) [21]. We demonstrated that addition of arginine to the C- or N-terminus of a peptide has a very small effect on the dissociation threshold. However, the dynamics of dissociation is dramatically affected by the presence of arginine. Selective fragmentation is characterized by a very large negative reaction entropy arising from the complex rearrangement process associated with this type of fragmentation.

This study is a continuation of the on-going research in our laboratory focused on the influence of acidic and basic residues on the energetics and dynamics of peptide fragmentation. Here we report on the energetics and dynamics of dissociation of singly protonated angiotensin II (DRVYIHPF) and its analogs (RVYIHPF, RVYIHAF and RVYIHDF). All peptides in this series contain a basic residue—arginine (R). Two of the peptides containing aspartic acid (D), DRVYIHPF and RVYIHDF, fragment via selective cleavages, while the other two peptides, RVYIHPF and RVYIHAF, fragment totally non-selectively.

2. Experimental

Surface-induced dissociation experiments were conducted on a specially fabricated 6T FT-ICR mass spectrometer. The instrument is equipped with a high-transmission electrospray source, consisting of an ion funnel interface [22] followed by three quadrupoles. The instrument is also fitted with a vacuum interlock assembly that allows the SID target to be positioned just inside the rear trapping plate of the ICR cell. Both the instrument and SID experimental protocol have been detailed elsewhere [23] and will be only briefly outlined below.

The SAM surface is positioned 1–2 mm inside of the rear trapping plate of the ICR cell. The surface is electrically connected to the rear trapping plate power supply. This ensures that the SAM surface and the rear trapping plate are at the same potential throughout the experiment. Ions are electrosprayed, at atmospheric pressure, into the end of a heated stainless steel capillary tube. The ion funnel that follows the capillary provides highly efficient ion transfer into the high vacuum region of the mass spectrometer. Three quadrupoles follow the ion funnel to provide collisional focusing, mass selection of the ion of interest and external accumulation of ions. Typical accumulation times are in the range of 0.3–0.8 s. The third (accumulation) quadrupole is held at an elevated pressure (2×10^{-3} Torr) for collisional relaxation of stored ions.

After accumulation, the ions are extracted from the third quadrupole, transferred into the ICR cell where they collide with the surface. Scattered ions are captured by raising the potentials on the front and rear trapping plates of the ICR cell by 10–20 V. Time-resolved mass spectra were acquired by varying the delay between the gated trapping and the excitation/detection event (the reaction delay). The reaction delay was varied from 1 ms to 1 s. Immediately following the fragmentation delay, ions were excited by a broadband chirp and detected. The collision energy is defined by the difference in the potential applied to the accumulation quadrupole and the potential applied to the rear trapping plate and the SID target. The ICR cell can be offset above or below ground by as much as ±150 V. Lowering the ICR cell below ground while keeping the potential on the third quadrupole fixed increases collision energy for positive ions.

Experimental control is accomplished with a MIDAS data station [24]. MIDAS is used to control the voltages and timing of the source and transfer optics, as well as ion manipulation in the ICR cell. An automated script was written to

allow for unattended acquisition of kinetic data. The script was used to vary the fragmentation delay and collision energy of the experiment. Reactions delays of 1, 10, 50 ms, 0.1, 0.3, and 1 s were studied. Typical experiments involved changing the collision energy across a relatively wide range from 15 to 65 eV. The automated script allowed for acquisition of SID spectra across the entire range of collision energies, in 1 eV increments, at each of the six fragmentation delays. Time dependent survival curves were constructed from experimental mass spectra by plotting the relative intensity of the precursor ion as a function of collision energy for each fragmentation delay.

The self-assembled monolayer (SAM) surface was prepared on a single gold {1 1 1} crystal (Monocrystals, Richmond Heights, OH, USA) using a standard procedure. The target was cleaned in a UV cleaner (Model 135500, Boekel Industries Inc., Feasterville, PA, USA) for 10 min and allowed to stand in a 1 mM ethanol solution of FC_{12} ($CF_3(CF_2)_9C_2H_4SH$), for 24–36 h. The target was removed from the SAM solution and ultrasonically washed in ethanol for 10 min to remove extra layers.

Angiotensin II (DRVYIHPF) and angiotensin III (RVYIHPF) were purchased from Sigma. Angiotensin analogs RVYIHAF and RVYIHDF were purchased from Peptron Inc. (Taejon, South Korea). All samples were dissolved in a 70:30 (v/v) methanol:water solution with 1% acetic acid. A syringe pump (Cole Parmer, Vernon Hills, IL, USA) was used for direct infusion of the electrospray samples at flow rates ranging from 20–50 $\mu l\,h^{-1}$.

2.1. RRKM modeling

The survival curves were modeled using an RRKM-based approach developed by our group [15,16]. For the modeling we separated time-dependent and time-independent fragments and used two dissociation rate constants for the total ion decomposition to account for the slow and fast fragmentation, as indicated schematically below:

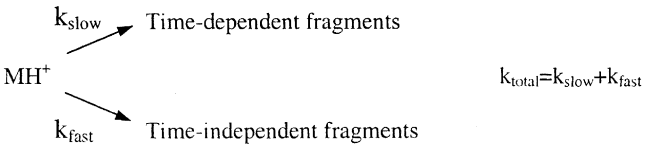

Microcanonical rate constants as a function of internal energy for the slow channel were calculated using the RRKM expression. For the fast reaction pathway the rate–energy dependence is very sharp and is best described by a step-function originating from the assumed threshold energy [19].

Fragmentation probability as a function of the internal energy of the parent ion and the experimental observation time (t_r), $F(E, t_r)$, is given by:

$$F(E, t_r) = e^{-(k_{total}(E)+k_{rad})t_r} \quad (1)$$

where k_{rad} is the rate constant for radiative cooling of the excited ion. The energy deposition function was described by the following analytical expression:

$$P(E, E_{coll}) = \frac{(E-\Delta)^l \exp(-(E-\Delta)/f(E_{coll}))}{C} \quad (2)$$

where l and Δ are parameters, $C = \Gamma(l+1)[f(E_{coll})]^{l+1}$ is a normalization factor and $f(E_{coll})$ has the form:

$$f(E_{coll}) = A_2 E_{coll}^2 + A_1 E_{coll} + A_0 \quad (3)$$

where A_0, A_1, and A_2 are parameters, and E_{coll} is the collision energy. Finally, the normalized signal intensity for a particular reaction channel is given by the equation:

$$I_i(E_{coll}) = \int_0^\infty F_i(E, t) P(E, E_{coll})\, dE \quad (4)$$

Collision-energy-resolved survival curves at different reaction times were constructed using the above procedure and compared to experimental data. The energy deposition function was kept the same for all reaction times. The fitting parameters were varied until the best fit to experimental curves was obtained. The fitting parameters included the critical energy and the activation entropy for the total decomposition of the precursor ion, the threshold for the fast fragmentation and parameters characterizing the energy deposition function (Eqs. (2) and (3)). The uniqueness of the fits was confirmed using sensitivity analysis described previously [16].

Vibrational frequencies of precursor ions were obtained from the frequency model given by Christie and co-workers [25]. Vibrational frequencies for the transition state were estimated by removing one C–N stretch (reaction coordinate) from the parent ion frequencies as well as varying all frequencies in the range of 500–1000 cm^{-1} to obtain the best fit with experimental data.

2.2. Molecular mechanics modeling

Molecular mechanics modeling of parent ion conformations was done using the Discover module of the Insight II software suite (Biosym Technologies, San Diego, CA, USA). The peptides were constructed using the amino acid library contained in the Biopolymer module. Both the N- and C-terminus of the peptide were capped with hydrogens and left neutral. The ionizing proton was then placed at the most basic sight (the N-terminus for LDIFSDF, and the arginine side chain for LDIFSDFR, RLDIFSDF, and LEIFSEFR). Using the Discover module the structures were subjected to a steepest descent minimization for 1500 iterations using the CFF91 force field. After minimization, the optimized structures were repeatedly annealed at 400 K for 1500 cycles. The resulting annealed structures were again minimized and the resulting minimized structure annealed again. The process was repeated until a local minimum was achieved and the intramolecular interactions could be observed. Intramolecular hydrogen bonding was observed by turning on the hydrogen

bonding feature of the program, using the default parameters, during the minimization and annealing (dynamics) experiments. All other parameters for the minimization and annealing were left at their default values. Approximately 15 structures obtained by repeated annealing/optimization were compared for each of the four peptides.

3. Results and discussion

3.1. Dissociation pathways

Surface-induced dissociation spectra for the four peptides—DRVYIHPF, RVYIHPF, RVYIHAF, and RVYIHDF—are shown in Fig. 1, while Table 1 lists all fragment ions observed in the range of collision energies used in SID experiments. All four spectra in Fig. 1 were acquired with a reaction delay (time between collision with the SAM surface and the excitation/detection event) of 1 s. The two peptides that do not contain acidic residues fragment totally non-selectively showing cleavages at almost every peptide bond. In contrast, the base peak in both of the aspartic acid (D) containing peptides, DRVYIHPF and RVYIHDF, is a fragment resulting from selective cleavages C-terminal to the aspartic acid, $\mathbf{y_7}$ and $\mathbf{b_6}$, respectively. Selective fragmentation of this kind is characteristic of peptides containing both acidic residues (aspartic or glutamic acids) and very basic residues (arginine or lysine) in the sequence. It has been demonstrated that selective fragmentation C-terminal to the acidic residue occurs when the number of ionizing protons is smaller or equal to the number of basic sites in the peptide [8].

The $\mathbf{y_7}$ fragment in the SID spectrum of DRVYIHPF is the result of selective cleavage C-terminal to the aspartic acid at position 1. Since it is the most basic site in the peptide, protonation likely takes place on the arginine side chain. The protonated side chain is then free to initiate cleavage C-terminal to the aspartic acid residue. The proton remains on the basic arginine side chain in the cleavage step and the $\mathbf{y_7}$ fragment is the detected product. The spectrum also contains a fragment of significant intensity resulting from the loss of water from the parent ion ($MH^+ - H_2O$). The remainder of the spectrum contains fragments resulting from non-selective fragmentation or successive fragmentation of $\mathbf{y_7}$ or $MH^+ - H_2O$ fragment ions.

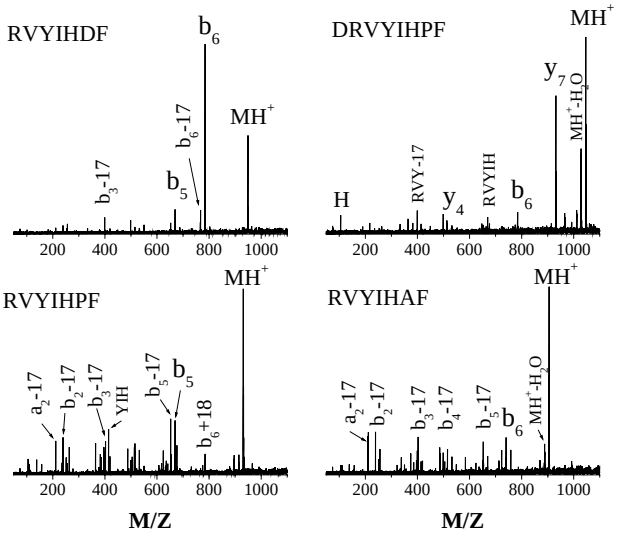

Fig. 1. Surface-induced dissociation spectra for RVYIHDF, 35.5 eV collision; DRVYIHPF, 39.5 eV collision; RVYIHPF 39.5 eV collision; RVYIHAF, 39.5 eV collision.

Singly protonated RVYIHDF contains both an arginine and an aspartic acid residues and fragments selectively. This selective fragmentation is indicated by the large intensity of the $\mathbf{b_6}$ ion (Fig. 1). It is interesting to note that the $\mathbf{b_6}$ fragment in the RVYIHDF spectrum is much larger than the $\mathbf{y_7}$ fragment in the spectrum of DRVYIHPF, even though both are selective cleavages resulting from the interaction of arginine and aspartic acid residues. A possible explanation is that the $\mathbf{y_7}$ ion in DRVYIHPF is formed in competition with the loss of water from the parent ion ($MH^+ - H_2O$). In contrast, the $\mathbf{b_6}$ ion from RVYIHDF has no competing loss of water from the parent ion and has higher intensity. The relative abundance of the $\mathbf{b_6}$ ion from RVYIHDF is similar to the summed relative abundance of the $\mathbf{y_7}$ and $MH^+ - H_2O$ ions from DRYVIHPF. Both the $\mathbf{y_7}$ and $MH^+ - H_2O$ ions from DRVYIHPF appear at the same collision energy, approximately 20 eV at a reaction time of 1 s, and are therefore in direct competition.

The spectra of both RVYIHPF and RVYIHAF are dominated by non-selective fragmentation. In both cases, the ionizing proton most likely resides on the highly basic side chain of the arginine residue. Since no acidic residues are present to direct cleavage, the protonated peptides decompose via non-selective fragmentation upon collision with the surface. For both peptides, mainly **b**-type fragment ions resulting from backbone cleavages with the proton remaining on the arginine residues at the N-termini are observed. Additional losses of NH_3 from many of the **b**-type ions are also observed in both peptides. A series of **y** ions (from $\mathbf{y_2}$ to $\mathbf{y_5}$) is observed for all peptides except for RVYIHDF. In addition, at higher collision energies several abundant immonium ions and small internal fragments (YIH, IH, HP, HD, HA) are observed. It should be noted that high-energy fragmentation of angiotensin II (data not shown) is very similar to fragmentation of RVYIHPF shown in Fig. 1. Indeed, the $\mathbf{y_7}$ ion resulting from DRVYIHPF is the same species as RYYIHPF. Consecutive fragmentation of the $\mathbf{y_7}$ ion of DRVYIHPF results in formation of the same fragment ions observed for RVYIHPF.

3.2. Results of molecular mechanics modeling

Molecular mechanics modeling was carried out on all four peptides to gain insight concerning interactions taking place within the protonated peptides. Fig. 2 shows the modeling

Table 1
List of SID fragments for different precursor ions

Sequence	N-terminal fragments	C-terminal fragments	Internal fragments	Immonium ions
RVYIHPF	a_1, a_2, a_3, a_4, a_5 **a_1^***, **a_2^***, a_3^*, **a_4^***, **a_5^*** **b_1**, b_2, b_3, **b_4**, **b_5** b_1^*, **b_2^***, **b_3^***, **b_4^***, **b_5^*** b_5^{**}, a_5^{**}, b_2^{**}, a_2^{**} $b_4 + H_2O$, $b_3 - H_2O$	y_1, **y_2**, **y_4**, **y_5**	b ions: **YIH**, **YIH − H_2O**, VYI, YI, **IH**, **HP** a ions: VYI*, IHP*, YI, IH, HP	**P**, **H**, Y
DRVYIHPF	a_5 a_3^* **b_2**, b_4, b_5, **b_6** **b_2^***, **b_3^***, b_4^* **$MH^+ - H_2O$**, **$MH^+ - 2H_2O$**	**y_2**, y_3, **y_4**, **y_7**	b ions: **RVYIH**, **RVYIH***, RVYI*, RVY, RVY*, **YIH**, YIH − H_2O, YI, RV, RV*, **IH**, **HP** a ions: RVYIH, RVYI, RVY, YI, IH, HP	**P**, **H**, Y, R
RVYIHDF	a_1, a_2, a_3, **a_4**, a_5 **a_1^***, **a_2^***, a_3^*, **a_4^***, a_5^* **b_1**, **b_2**, b_3, **b_4**, **b_5**, **b_6** b_1^*, **b_2^***, **b_3^***, **b_4^***, **b_5^***, **b_6^*** **$b_4 + H_2O$**, $b_3 - H_2O$	y_1, y_2, y_3	b ions: YIH, IHD, YI, VY, **IH**, **HD** a ions: YI, IH, VY	**H**, Y
RVYIHAF	a_1, a_2, a_3, a_4, a_6 **a_1^***, **a_2^***, **a_4^***, a_5^* **b_1**, **b_2**, b_3, **b_4**, **b_5**, **b_6** b_1^*, **b_2^***, **b_3^***, **b_4^***, **b_5^***, **b_6^*** **$b_6 + H_2O$**, $b_3 - H_2O$, **$MH^+ - H_2O$**	y_1, **y_3**, y_5	b ions: **YIHA**, YIH, IHA, YI, VY, **IH**, **HA** a ions: YI, IH, HA	R, **H**, Y

*Denotes loss of NH_3 from the corresponding fragment. Major peaks are highlighted with bold letters.

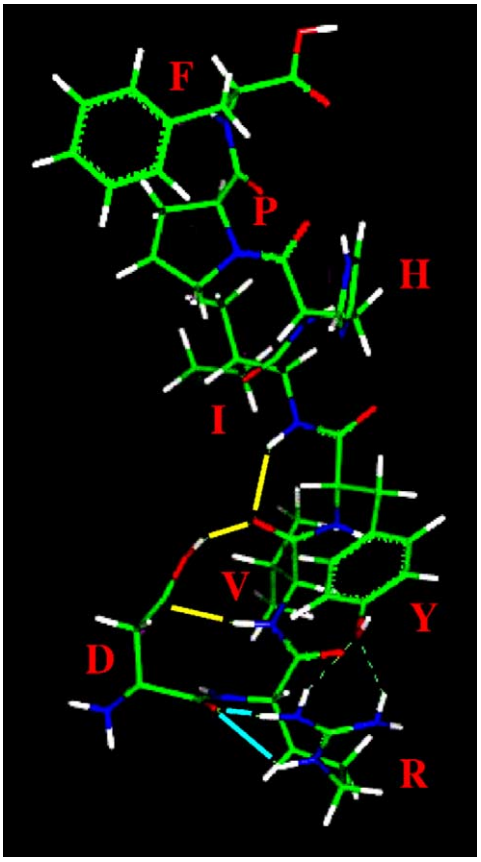

Fig. 2. Optimized structure of singly protonated DRVYIHPF from molecular mechanics modeling. Interactions discussed in the text are highlighted with light blue and yellow lines.

results for DRVYIHPF. This peptide ion assumes an elongated conformation, with most of the internal interactions taking place in the N-terminal part of the peptide containing residues 1–4 (DRVY). The carbonyl oxygen between the aspartic acid residue and the arginine residue is interacts strongly with the protonated arginine side chain (light

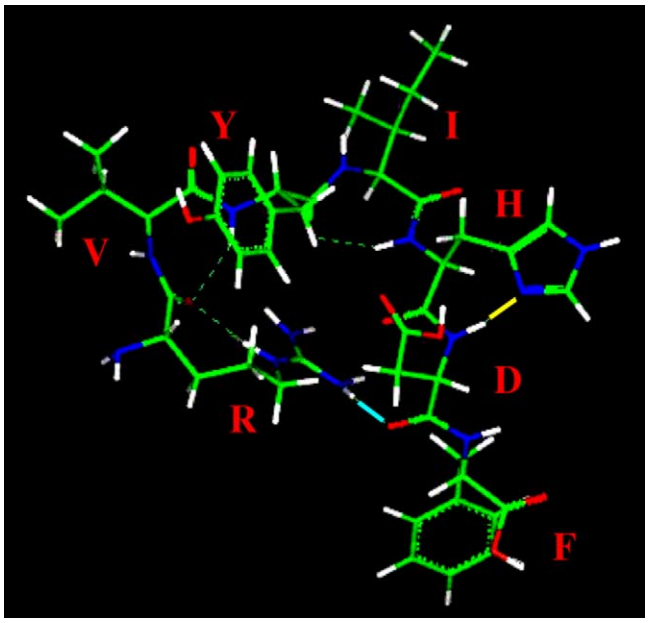

Fig. 3. Optimized structure of singly protonated RVYIHDF from molecular mechanics modeling. Interactions discussed in the text are highlighted with light blue and yellow lines.

blue lines in Fig. 2). This interaction promotes cleavage C-terminal to the aspartic acid, accounting for the large $\mathbf{y_7}$ fragment ion observed in the spectrum. In addition to the interaction with arginine, the side chain of the aspartic acid residue participates in H-bonding with the carbonyl oxygens (yellow line) between the residues in positions 2 and 3 (R-V) and positions 4 and 5 (Y-I) (Fig. 2).

The other peptide that undergoes decomposition by selective cleavage, RVYIHDF (Fig. 3), also shows an interaction between the protonated arginine side chain and the carbonyl oxygen C-terminal to the aspartic acid residue (light blue line). Selective cleavage C-terminal to the aspartic acid results in the large $\mathbf{b_6}$ ion observed in the SID spectrum (Fig. 1). There is no direct interaction between the arginine and the aspartic acid side chain analogous to that observed for DRYVIHPF. This absence of direct interaction with the aspartic acid side chain may be the reason that water loss from the parent ion is not observed.

Molecular mechanics modeling also predicts an interaction between the amine of the peptide bond on the N-terminal side of the aspartic acid with the side chain of the histidine residue (yellow line). This rationalizes the formation of the $\mathbf{b_5}$ ion when RVYIHDF is a precursor. Since histidine is known to direct cleavage C-terminal to itself when protonated [5], it is possible that the formation of $\mathbf{b_5}$ fragment ion is the result of proton transfer from the arginine to the histidine residue followed by dissociation. If the histidine residue were protonated, the proton would most likely reside on the nitrogen in position three of the histidine side chain ring. The protonated side chain could then interact with the carbonyl group of the peptide bond C-terminal to the histidine residue. Cleavage could then occur at the peptide bond following an intramolecular proton transfer between the histidine side chain and carbonyl group of the H–D peptide bond.

The remaining peptides, RVYIHPF and RVYIHAF, do not contain an aspartic acid and therefore do not undergo selective cleavages. Their spectra are dominated by backbone cleavages (see Fig. 1). Molecular mechanics modeling (not shown) of both peptides shows numerous interactions between the basic arginine side chain and other peptide bonds within the peptide chains rationalizing the extensive backbone fragmentation observed for these ions.

3.3. Kinetic studies

Kinetic experiments were conducted by changing the time delay between ion impact and the detection event from 1 ms to 1 s. Comparison of the survival curves for all four peptides at reaction times of 1 ms and 1 s is shown in Fig. 4. With increase in reaction time the amount of internal energy needed for fragmentation (the kinetic shift) decreases; this is reflected in corresponding shifts in survival curves to lower collision energies. It is also interesting to note that the shapes of survival curves and their time behavior are quite different for the four peptides. At 1 ms reaction time all curves are steep, indicating that fragmentation is quite fast. Survival curves for RVYIHPF, RVYIHDF and RVYIHAF overlap at this reaction time. Based on results obtained at 1 ms delay time it seems that these three peptides have approximately the same stability, while DRVYIHPF is somewhat more stable. However, shapes of survival curves of the two peptides that undergo selective fragmentation obtained with 1 s reaction time are dramatically different. Specifically, survival curves for RVYIHDF and DRVYIHPF are very shallow and the onset for dissociation is substantially lower for these two peptides as compared to RVYIHPF and RVYIHAF. This dramatic effect of the reaction time on the shape and position of the survival curve results from significant entropy differences for selective and non-selective fragmentation.

Close examination of the position of survival curves shown in Fig. 4 reveals that fragmentation of aspartic acid-containing peptides (RVYIHDF and DRVYIHPF), i.e., selective fragmentation, is characterized by lower threshold energy than dissociation via non-selective pathways

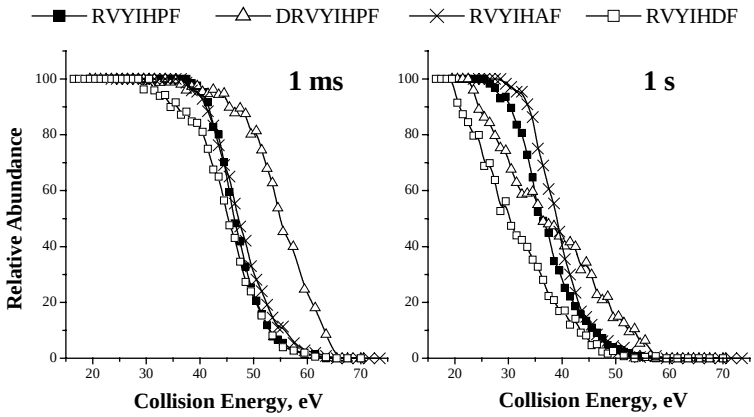

Fig. 4. Fragmentation efficiency curves for RVYIHPF (filled squares), DRVYIHPF (open triangles), RVYIHAF (crosses), and RVYIHDF (open squares) at reaction delays of 1 ms (left panel) and 1 s (right panel).

(RVYIHPF and RVYIHAF). The shapes of the curves at 1 s are characteristic of the reaction entropy. Kinetically unfavored reactions with large negative reaction entropy are associated with shallow survival curves, while fast (kinetically favored) fragmentation results in steep survival curves. Shallow curves obtained for RVYIHDF and DRVYIHPF at 1 s reaction time indicate that selective fragmentation is characterized by large negative activation entropy, while relatively fast fragmentation occurs when a peptide fragments non-selectively.

The dramatic change in the shapes of the curves for RVYIHDF and DRVYIHPF with reaction time can be rationalized by considering competition between slow RRKM-type fragmentation and instantaneous fragmentation of ions on the surface (shattering). We have shown that shattering of peptide ions on surfaces becomes dominant at high collision energies and short reaction times [19]. Steepness of survival curves for RVYIHDF and DRVYIHPF at 1 ms reaction time indicates that shattering is the major fragmentation mechanism for these peptide ions on a short timescale. An important conclusion deduced from Fig. 4 is that it is not possible to access relative stability of large peptide ions based on the energy-resolved results obtained at a single reaction delay. This is particularly important for short reaction times because dissociation on a microsecond timescale is often dominated by shattering and the energy dependence of the relative abundance of the precursor ion on ion kinetic energy does not reflect its stability if this is the case.

A good measure of the relative amounts of energy required to observe fragmentation at different timescales is the value of $E_{50\%}$, i.e., the collision energy, at which fragmentation efficiency equals 50%. Time dependence of the values of $E_{50\%}$ for all four peptides is summarized in Fig. 5. The dramatic decrease in $E_{50\%}$ from short to long times, followed by the gradual leveling off, is very similar to that reported in previous studies [21]. The leveling off in these curves results from competition between dissociation and radiative cooling of excited precursor ions. The $E_{50\%}$ curves of RVYIHPF, RVYIHAF are very similar and show a smaller shift in the values of $E_{50\%}$ as a function of time as compared to the pair of peptides that fragment selectively. Slower dissociation results in a more dramatic decrease in $E_{50\%}$ as a function of reaction time. Shifts in the $E_{50\%}$, of 16.4, 11.5, 9.4, and 15.9 eV for DRVYIHPF, RVYIHPF, RVYIHAF, and RVYIHDF, respectively, were observed by changing the reaction delay from 1 ms to 1 s. The observed shifts are consistent with qualitative conclusions made earlier, namely, that decomposition via selective cleavages is entropically less favorable than decomposition via non-selective pathways.

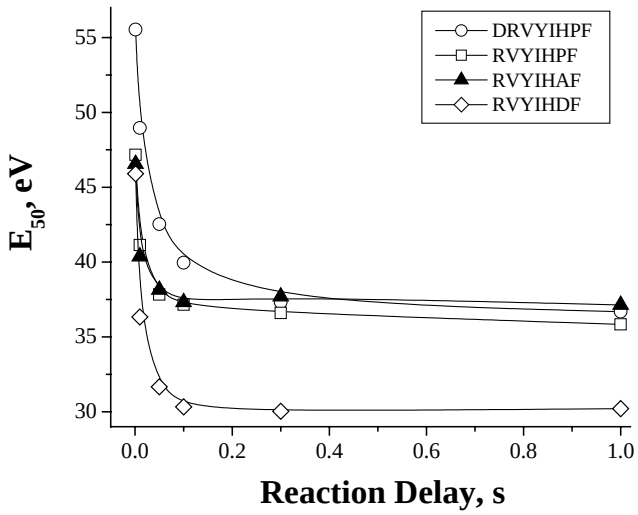

Fig. 5. Time dependence of the collision energy required to observe 50% fragmentation of the precursor ion ($E_{50\%}$) for DRVYIHPF (open circles), RVYIHPF (open squares), RVYIHAF (filled triangles), and RVYIHDF (open diamonds).

3.4. RRKM modeling of experimental data

Quantitative description of the kinetics of decomposition of angiotensin analogs was obtained by modeling the experimental survival curves using the RRKM based method outlined earlier. Fig. 6 shows the results of the RRKM modeling for all four peptides, while the corresponding dissociation parameters are summarized in Table 2. (It should be noted that dissociation parameters listed in Table 2 represent an average over all dissociation channels.) Symbols in Fig. 6 represent experimental points obtained at fragmentation delays of 1, 10, 50 ms, and 1 s, while modeling results are shown as solid lines. There is a good agreement between experimental and simulated results. Dashed lines in Fig. 6 were obtained by blocking the fast fragmentation channel to represent the relative contribution of slow fragmentation to the total decomposition of the precursor ion. Microcanonical rate–energy dependences for all four ions are shown in Fig. 7. We shortly discuss the results of RRKM modeling and compare them to our previous study of peptides containing LDIFSDF motif [21].

In our previous study we examined the effect of addition of an arginine residue on dissociation of peptides containing acidic residues. We found that addition of a basic residue to peptides containing aspartic acid results in a very small increase in the dissociation threshold, while the dynamics of dissociation is affected dramatically. Threshold energies of 1.24 and 1.31 eV were reported for selective fragmentation of LDIFSDFR and RLDIFSDF, respectively, indicating a small but measurable effect of the position of the basic amino acid on the fragmentation energetics. Pre-exponential *A*-factors for selective fragmentation were at least two orders of magnitude lower than the *A*-factor for non-selective fragmentation (4.8×10^{11} and 3.3×10^{11} s^{-1} for LDIFSDFR and RLDIFSDF, respectively, as compared to 2.1×10^{13} s^{-1} for LDIFSDF).

In the present study we examined the effect of addition of an acidic residue (aspartic acid) on dissociation of arginine-containing peptides. Table 2 shows that addition of the aspartic acid to peptide sequence has a dramatic effect

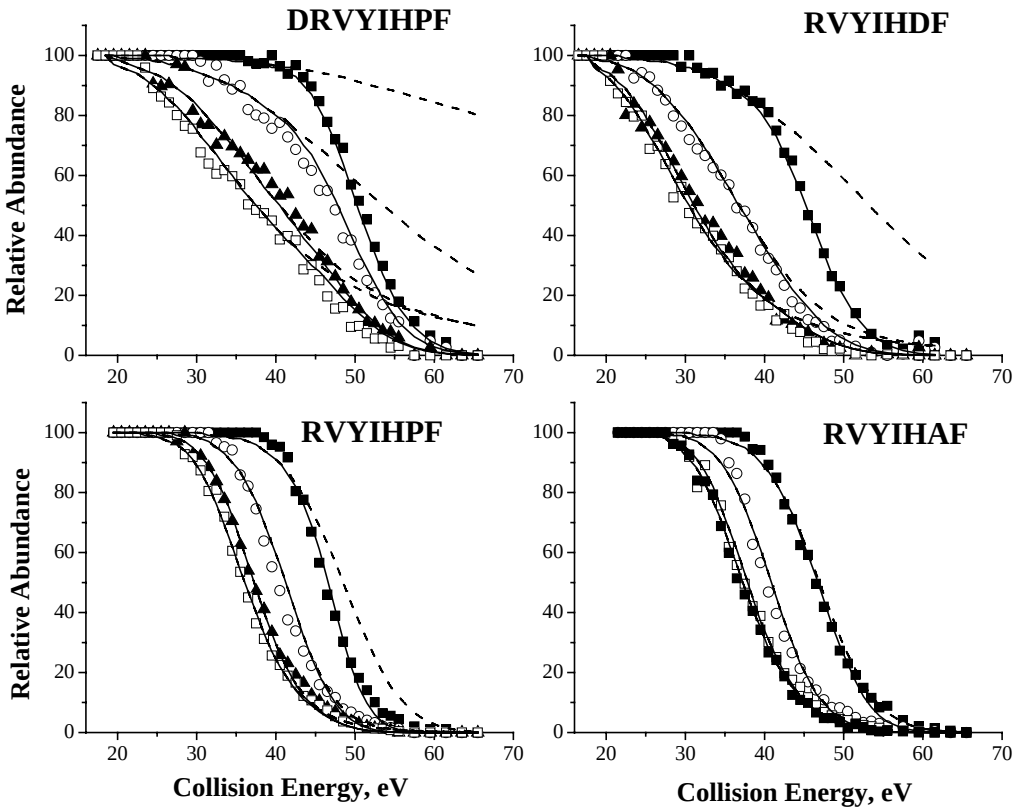

Fig. 6. RRKM modeling results fit to time resolved survival curves for DRVYIHPF, RVYIHDF, RVYIHPF, and RVYIHAF. The modeling results taking into account slow and fast dissociation channels are represented by solid lines while the points represent the experiment survival curves for reaction delays of 1 ms (filled squares), 10 ms (open circles), 50 ms (filled triangles), and 1 s (open squares). Dashed lines represent the contribution of the slow decay channel to the total decomposition of the parent ion.

on both the threshold energy and the dissociation entropy. Threshold energies for peptide ions that do not contain the aspartic acid and therefore undergo non-selective fragmentation are almost 0.5 eV higher than the values characteristic of selective fragmentation. There is also a 3–4 orders of magnitude difference in pre-exponential factors characteristic of non-selective (8.2×10^{11} and $7.2 \times 10^{12}\ s^{-1}$ for RVYIHPF and RVYIHAF, respectively) and selective (3.1×10^{8} and $5.0 \times 10^{7}\ s^{-1}$ for RVYIHDF and DRVYIHPF, respectively).

Dissociation threshold obtained for selective fragmentation (1.14 eV) is close to but slightly lower than the previously published values of 1.24 eV for LDIFSDFR and 1.31 eV for RLDIFSDF, while pre-exponential factors obtained for selective fragmentation of angiotensin analogs are significantly lower than the corresponding values obtained for LDIFSDFR and RLDIFSDF. However, similar relative differences between pre-exponential factors for selective and non-selective fragmentation were obtained for the two different series of peptides. Specifically, transition from non-selective to selective fragmentation is characterized by a 3–4 orders of magnitude decrease in the pre-exponential factor.

Table 2
Results of the RRKM modeling of the precursor ion survival curves (uncertainties are shown in parentheses)

	RVYIHPF	RVYIHAF	RVYIHDF	DRVYIHPF
E_0 (eV)	1.62 (0.03)	1.62 (0.05)	1.14 (0.03)	1.13 (0.03)
$\Delta S^{\ddagger}$ (cal mol^{-1} K^{-1})	−7.0 (0.3)	−2.72 (0.6)	−22.7 (0.5)	−26.3 (0.5)
A (s^{-1})	8.2×10^{11}	7.2×10^{12}	3.1×10^{8}	5.0×10^{7}
E_{fast} (eV)	12.0 (0.4)	11.5 (0.7)	11.3 (0.5)	11.9 (0.7)
T → V transfer (%)	21.9 (0.8)	19.8 (1.5)	21.2 (0.9)	20.5 (1.2)
k_{rad} (s^{-1})	14	21	25	15
DOF	396	384	393	435
KS ($t = 1$ s) (eV)	6.3	5.9	4.2	5.0

E_0 is the threshold energy, $\Delta S^{\ddagger}$ is the entropy change for the transition state, A is the pre-exponential factor at 500 K, E_{fast} is the threshold for shattering; T → V transfer (%) is the percentage of the ion's kinetic energy converted to internal energy upon collision, k_{rad} is the radiative decay rate, DOF is the number of vibrational degrees of freedom, and KS ($t = 1$ s) is the kinetic shift at 1 s fragmentation delay.

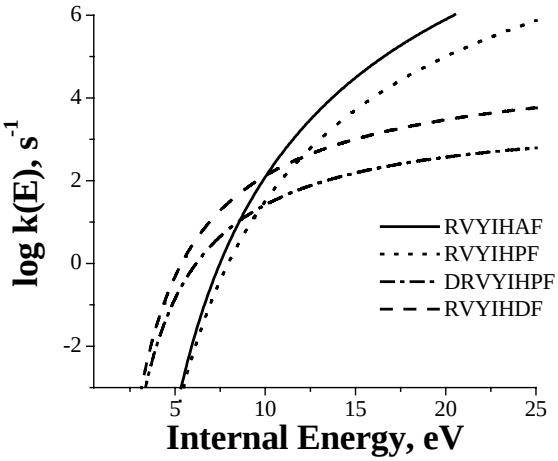

Fig. 7. Semilogarithmic plot of microcanonical rate–energy dependences for DRVYIHPF (dashed dotted line), RVYIHDF (dashed line), RVYIHPF (dotted line), and RVYIHAF (solid line).

The relative position of the acidic and basic residues in RVYIHDF and DRVYIHPF does not affect the dissociation threshold but has a measurable effect on the dissociation entropy. Slower fragmentation is observed when the aspartic acid residue is located at the N-terminus (DRVYIHPF). We infer that this difference reflects differences between entropy effects for the cleavage C-terminal to aspartic acid and the loss of water from the peptide, the dominant competitive reaction channel for DRVYIHPF. No competitive water loss was observed for RVYIHDF. Because in this study we modeled only the total decomposition rate for each peptide ion, the presence of a second dissociation channel in competition with the selective cleavage C-terminal to aspartic acid is the most probable cause of the differences in dissociation entropies for the total decomposition of RVYIHDF and DRVYIHPF. A similar difference in entropy effects is reported for dissociation of RVYIHPF and RVYIHAF. Namely, replacing proline with alanine results in a 10-fold increase in dissociation rate, while the dissociation threshold remains the same. Because dissociation patterns for these two peptides are very similar, this entropy effect reflects the influence of secondary structure of the peptide on the dissociation entropy.

It is important to note that these relatively small differences between dissociation parameters can be accurately evaluated from our experimental data. This results from the significant amplification that occurs in SID experiments for large peptides described in our previous studies [19–21]. The amplification results from two factors: the kinetic shift observed for large peptides even on a long timescale of FT-ICR experiments and the fact that only a fraction of the collision energy is converted into internal excitation of precursor ions. The values for kinetic shifts listed in Table 2 provide a clear indication of such amplification. Small differences in reaction entropies are translated into 0.4 eV difference in kinetic shifts for RVYIHPF and RVYIHAF and 0.8 eV difference for RVYIHDF and DRVYIHPF. The differences in kinetic shifts are further supported by microcanonical rate–energy dependences shown in Fig. 7. Although rate–energy dependences for each pair of peptides (RVYIHPF/RVYIHAF and RVYIHDF/DRVYIHPF) have the same origin they display significant deviation at higher internal energies because of differences in reaction entropies. Further, because only ca. 20% of ion kinetic energy is converted into the internal energy of the ion, these values are multiplied by a factor of 5 to give 2 and 4 eV shifts in survival curves for the RVYIHPF/RVYIHAF pair and RVYIHDF/DRVYIHPF pair, respectively. We have previously demonstrated this two-step amplification for accurate measurement of small differences in dissociation thresholds of large ions using FT-ICR SID experiments [21]. In this study the same concept is demonstrated for the situation when small differences between reaction entropies are measured experimentally.

Dissociation thresholds obtained for non-selective fragmentation are higher than values reported by us previously for arginine-containing peptides of similar size. In addition to threshold energies for LDIFSDFR and RLDIFSDF listed above, we have established dissociation thresholds of 1.17 and 1.09 eV for des-Arg^1- and des-Arg^9-bradykinin (PPGFSPFR and RPPGFSPF), respectively [19]. Although these peptides do not contain the aspartic acid residue their fragmentation is also very selective at low collision energies. Significantly larger values obtained in this study for RVYIHAF and RVYIHPF are in a general agreement with the "mobile proton" model that suggests that the dissociation energy increases when arginine is present in peptide sequence. However, our observations also indicate a strong influence of the reaction entropy on dissociation of large ions. Although non-selective fragmentation of the angiotensin analogs is associated with much higher pre-exponential factors than selective fragmentation, it is still fairly slow when compared to peptides containing the LDIFSDF motif.

The calculated values of kinetic shifts for 1 s reaction delay are listed in Table 2 along with the number of vibrational degrees of freedom (DOF) for each ion. Because of the significantly different entropy factors for dissociation, there is no correlation between the excess internal energy required to observe dissociation and the number of DOF. This observation is important because it is commonly assumed that a simple linear correction for the DOF effect can be applied to collision-energy-resolved data [8]. This assumption is strictly correct only for reactions that are characterized by the same entropy effects. We have previously demonstrated that reaction entropies associated with peptide fragmentation in the gas phase show substantial variations as a function of both the primary and secondary peptide structure. The DOF correction should therefore not be used unless there are independent measurements demonstrating very similar entropies of dissociation for the reactions being compared.

Dashed lines in Fig. 6 represent the relative contribution of the slow unimolecular decomposition to the overall decay of the precursor ion as a function of collision energy and reaction time. Similarly to our previous studies fast

fragmentation becomes significant for short reaction times and high collision energies. This fragmentation is modeled in the "sudden death" approximation and represents instantaneous fragmentation of ions during their collision with the surface (shattering). The average value of the shattering threshold obtained for angiotensin analogs is 11.5 eV. The smallest contribution of shattering to the total decomposition of the precursor ion is observed for RVYIHAF—the peptide ion with the highest dissociation entropy in this series. A somewhat larger effect is observed for RVYIHPF, for which simulated survival curves with and without contribution of the fast decay deviate at 1 ms reaction delay. However, for the two peptides that fragment selectively the contribution of shattering is very significant. It accounts for more than 50% decomposition of RVYIHDF and for more than 80% decomposition of DRVYIHPF at 1 ms reaction delay. This clearly explains the dramatic variation in the shapes of survival curves as a function of reaction delay observed for these two ions discussed earlier. Specifically, the steepness of the survival curve for DRVYIHPF at 1 ms delay time results from shattering. The curve at 10 ms delay shows a clear break in the slope as a function of collision energy—at low collision energy the slope reflects slow statistical decay while at higher collision energy fast decay is dominant. Similar changes in the slope are observed for the 1 ms survival curve of RVYIHDF. Finally, at long reaction times the relative contribution of the fast decay process is relatively small and the shape of the curve is determined mainly by the slow decay rate.

4. Conclusions

In this work we have utilized time- and energy-resolved SID experiments to establish the energetics and dynamics of dissociation of large peptide ions containing arginine and aspartic acid residues. Because collision-energy-resolved SID data are very sensitive to both the energetics and dynamics of dissociation accurate dissociation parameters can be obtained from these experiments. This sensitivity results from an efficient amplification of differences in dissociation parameters. Two factors contribute to the amplification: the substantial kinetic shift obtained for large molecules even on a long timescale and the T → V conversion efficiency, close to 20% for peptides studied in this work. SID conversion efficiency provides an additional factor of 5 amplification of the differences in the internal energies required to observe dissociation on the experimental timescale. In addition, measuring the time dependence of the precursor ion survival curve imposes serious constraints on the RRKM-based modeling results. This allows an efficient separation of energy and entropy effects on the survival curves.

The series of peptides studied in this work can be divided into two pairs: peptides that fragment non-selectively (RVYIHPF and RVYIHAF) and peptides that undergo selective fragmentation (RVYIHDF and DRVYIHPF). Addition of the aspartic acid residue to peptide sequence resulting in transition from non-selective to selective fragmentation is associated with a substantial (ca. 0.5 eV) reduction in the dissociation energy and 3–4 orders of magnitude reduction in the pre-exponential factor. The difference between entropy factors for selective and non-selective fragmentation indicate that selective cleavages are associated either with substantial rearrangements or require a very specific conformation in order to undergo dissociation. In addition small entropy effects within each pair of peptides was observed. We found that the relative position of the acidic and basic residues in RVYIHDF and DRVYIHPF do not affect the dissociation threshold but rather have a measurable effect on the dissociation entropy. This effect was attributed to the presence of a competing water loss channel that contributes to the total decomposition of DRVYIHPF that is not observed for RVYIHDF. In contrast, an order of magnitude difference in pre-exponential factors for dissociation of RVYIHAF and RVYIHPF was attributed to the influence of the secondary peptide structure on the dissociation dynamics.

Similarly to our previous studies we modeled the total decomposition of the precursor ion using two decay rates: slow unimolecular fragmentation of the excited precursor ion scattered off the surface and fast instantaneous decay on the surface (shattering). The largest contribution of the fast decay was observed for ions that undergo selective fragmentation. The fast decay has a strong effect on the shape of the parent ion survival curve and its evolution as a function of reaction time. Specifically, more than 80% fragmentation of DRVYIHPF at 1 ms is caused by shattering. Because dissociation is very fast a steep survival curve is obtained for this ion at 1 ms reaction delay. With increase in reaction time the contribution of the fast decay rapidly decreases. The overall shape of survival curves at long reaction delay is determined by the slow decay rate. These observations are particularly important because they strongly suggest that it is not possible to access relative stability of large peptide ions based on the energy-resolved results obtained at a single reaction delay. Great caution should be taken when energy dependence of fragmentation of large ions is examined on a microsecond timescale. For short reaction times dissociation is likely dominated by shattering and the energy dependence of the relative abundance of the precursor ion does not reflect its stability.

Acknowledgements

All of the work described herein was conducted at the W.R. Wiley Environmental Molecular Sciences Laboratory (EMSL), a national scientific user facility sponsored by the US Department of Energy and located at Pacific Northwest National Laboratory. PNNL is operated by Battelle for the US Department of Energy. Financial support for T.H.B.

was provided through NSF grant CHE-9634238. Research at EMSL was carried out within the project 40457 supported by the Office of Basic Energy Sciences of the US Department of Energy.

References

[1] O. Burlet, C.Y. Yang, S.J. Gaskell, J. Am. Soc. Mass Spectrom. 3 (1992) 337.
[2] O. Burlet, R.S. Orkiszewski, K.D. Ballard, S.J. Gaskell, Rapid Commun. Mass Spectrom. 6 (1992) 658.
[3] A.R. Dongre, J.L. Jones, A. Somogyi, V.H. Wysocki, J. Am. Chem. Soc. 118 (1996) 8365.
[4] M.J. Polce, D. Ren, C. Wesdemiotis, J. Mass Spectrom. 35 (2000) 1391.
[5] V.H. Wysocki, G. Tsaprailis, L.L. Smith, L.A. Breci, J. Mass Spectrom. 35 (2000) 1399.
[6] A. Schlosser, W.D. Lehmann, J. Mass Spectrom. 35 (2000) 1382.
[7] R.A.J. O'Hair, J. Mass Spectrom. 35 (2000) 1377.
[8] G. Tsaprailis, H. Nair, A. Somogyi, V.H. Wysocki, W. Zhong, J.H. Futrell, S.G. Summerfield, S.J. Gaskell, J. Am. Chem. Soc. 121 (1999) 5142.
[9] W. Yu, J.E. Vath, M.C. Huberty, S.A. Martin, Anal. Chem. 65 (1993) 3015.
[10] J. Qin, B.T. Chait, J. Am. Chem. Soc. 117 (1995) 5411.
[11] S.G. Summerfield, A. Whiting, S.J. Gaskell, Int. J. Mass Spectrom. Ion Processes 162 (1997) 149.
[12] G. Tsaprailis, A. Somogyi, E.N. Nikolaev, V.H. Wysocki, Int. J. Mass Spectrom. 195/196 (2000) 467.
[13] C. Lifshitz, Eur. J. Mass Spectrom. 8 (2002) 85.
[14] T. Baer, W.L. Hase, Unimolecular Reaction Dynamics, Theory and Experiments, Oxford University Press, NY, 1996.
[15] J. Laskin, M. Byrd, J.H. Futrell, Int. J. Mass Spectrom. 196 (2000) 285.
[16] J. Laskin, J.H. Futrell, J. Phys. Chem. A 104 (2000) 5484.
[17] J. Laskin, E. Denisov, J.H. Futrell, J. Am. Chem. Soc. 122 (2000) 9703.
[18] J. Laskin, E. Denisov, J.H. Futrell, Int. J. Mass Spectrom. 219 (2002) 189.
[19] J. Laskin, T.H. Bailey, J.H. Futrell, J. Am. Chem. Soc. 125 (2003) 1625.
[20] J. Laskin, Eur. J. Mass Spectrom. 10 (2004) 259.
[21] T.H. Bailey, J. Laskin, J.H. Futrell, Int. J. Mass Spectrom. 222 (2002) 312.
[22] S.A. Shaffer, K. Tang, G.A. Anderson, D.C. Prior, H.R. Udseth, R.D. Smith, Rapid Commun. Mass Spectrom. 11 (1997) 1813.
[23] J. Laskin, E.V. Denisov, A.K. Shukla, S.E. Barlow, J.H. Futrell, Anal. Chem. 74 (2002) 3255.
[24] M.W. Senko, J.D. Canterbury, S. Guan, A.G. Marshall, Rapid Commun. Mass Spectrom. 10 (1996) 1839.
[25] P.J. Derrick, P.M. Loyd, J.R. Christie, in: I. Cornides, G. Howárth, K. Vékey (Eds.), Advances in Mass Spectrometry, vol. 13, Wiley, Chichester, 1995.